Polymer Journal (2018) 50:775–786
https://doi.org/10.1038/s41428-018-0076-0

ORIGINAL ARTICLE

Nucleation effects of high molecular weight polymer additives on low molecular weight gels

Symone L. M. Alexander[1,2] · LaShanda T. J. Korley[2,3]

Received: 1 February 2018 / Revised: 10 April 2018 / Accepted: 11 April 2018 / Published online: 21 May 2018

Abstract

Polymeric species have been introduced to low molecular weight gelators to tailor their nucleation and rheological behavior. This work combines polymers and molecular gels (MGs) in a different manner by using polymers as the major component in a solution. Additionally, using polymers above their entanglement molecular weight is a step towards building polymer–MG composite materials. Specifically, a cholesterol-pyridine (CP) molecular gel was introduced to poly(ethylene oxide-*co*-epichlorohydrin) (EO-EPI) and poly(vinyl acetate) (PVAc), which have dissimilar chain conformations in anisole. Dynamic light scattering, scanning electron microscopy, and temperature-dependent small- and wide-angle X-ray studies were utilized to investigate the influence of the solution properties of high molecular weight EO-EPI and PVAc on the CP network structure. The collapsed chain conformation and aggregation of EO-EPI led to isolated, branched CP fiber networks, resulting in unexpectedly high dissociation temperatures. In contrast, PVAc gels displayed transient fiber networks, as evidenced by fiber wrapping and bundling. Cooperative interactions between PVAc and CP resulted in gels with dissociation temperatures higher than those of pure CP gels. These structural characteristics significantly influenced the gel mechanics. The collapsed chain conformation of EO-EPI led to weaker, more viscous gels, and the freely extended PVAc chain conformation led to interconnected, elastic gels independent of the molecular gel concentration.

Introduction

Material properties can be developed and refined through a fundamental understanding of nanoscale assembly. For example, self-assembling fiber structures have been utilized to reinforce or introduce stimuli-responsive behavior to polymer nanocomposites. Polymer nanocomposites can incorporate nanoscale additives in polymer matrices in order to enhance the properties of the matrix material. Cellulose nanowhiskers, carbon nanotubes, and electrospun nanofibers have all been employed as nanoscale additives that result in mechanical reinforcement or switchability [1–6]. For example, Cudjoe et al. recently fabricated biomimetic, thermally driven polymer nanocomposites with polymer-grafted cellulose nanocrystals (CNCs) as reversibly responsive fillers in a poly(vinyl acetate) matrix [7]. The lower critical solution temperature (LCST) polymers reversibly controlled the assembly of the CNCs within the composite, which strengthened or weakened the polymer nanocomposite as a function of temperature. Additionally, carbon nanotubes have been utilized to enhance the mechanical and responsive properties of commodity polymers, such as polyurethanes [8]. Though these rigid, nanoscale fillers can produce mechanically enhanced materials, they are hindered by concentration and mixing thresholds that induce aggregation and separation from the polymer matrix [9, 10]. An alternative approach to preformed fibers or particles is to utilize the non-covalent interactions of self-assembling small molecules to generate a structural hierarchy. The use of small molecules may combat many of the challenges of aggregation and delamination observed in traditional, fiber-reinforced composites.

Electronic supplementary material The online version of this article (https://doi.org/10.1038/s41428-018-0076-0) contains supplementary material, which is available to authorized users.

✉ LaShanda T. J. Korley
lkorley@udel.edu

[1] Department of Macromolecular Science and Engineering, Case Western Reserve University, Cleveland, OH 44106, USA

[2] Department of Materials Science and Engineering, University of Delaware, Newark, DE 19716, USA

[3] Department of Chemical and Biomolecular Engineering, University of Delaware, Newark, DE 19716, USA

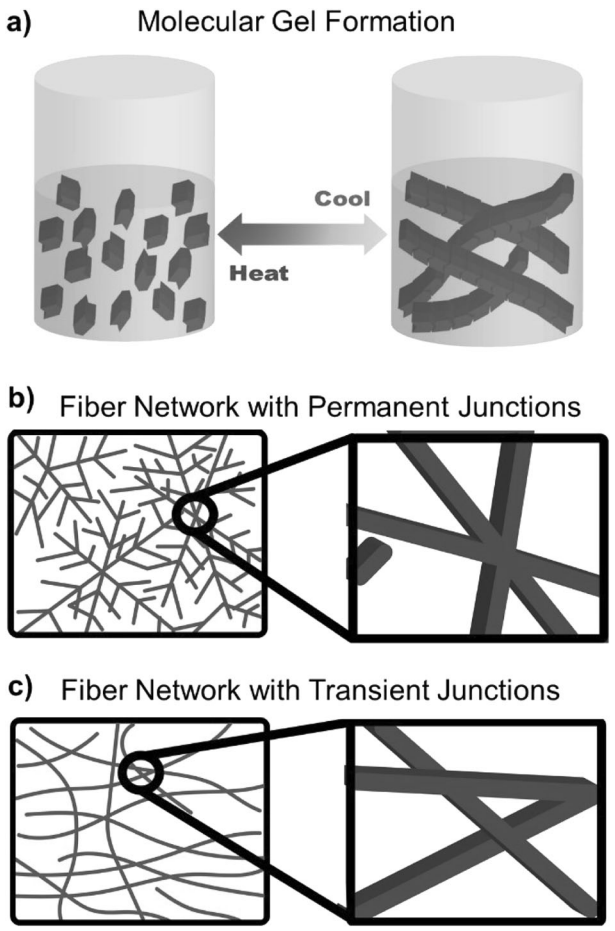

Fig. 1 Schematic representations of the molecular gel formation and network structures. **a** Molecular gel formation, **b** fiber network with permanent junctions, and **c** fiber network with transient junctions

Small molecules that can form long-range assemblies can be easily incorporated into a wide range of systems, allowing complex behaviors to be achieved from simple designs. Previously, our group developed a UV-polymerizable diacetylene small molecule filler, which was utilized to form a mechanically enhanced composite [11]. Incorporation of diacetylene MG as a self-assembling small molecule additive resulted in a 2-fold increase in strength compared to that of the original polymer matrix. Low molecular weight gels or molecular gels (MGs) can reversibly trap solvents in their self-assembled networks (Fig. 1a) [12]. A variety of MGs have been discovered utilizing existing small molecules, such as amino acids and sugar derivatives [13, 14], or have been synthetically designed. The simplest method of gelation is thermally driven [12], but gelation has also been induced via UV exposure [15], pH [16], ionization [17], perturbation [18], and solvent exchange [19]. In thermal gelation, the MG is heated until it dissolves, and rather than recrystallizing upon cooling, it forms a gel (Fig. 1a). Thus, the process of gelation is a balance between solubilization and crystallization. This process is driven by solvent-MG interactions and the nucleation of the molecular gel into long-range networks of fibers, platelets, or coagulated spheres [12].

The structural requirements and assembly modes of molecular gels have been extensively examined [20–25]. Li et al. presented descriptions of nucleation modes that result in either permanent or transient junctions connected by fibers [26]. Realistically, a gel network rarely consists of either purely permanent or purely transient junctions. Even so, the predominately occurring junction type determines the strength and rheological behavior of the entire network. Permanent junctions are evidenced by branching from either the sides or tips of growing fibers, and this process results in materials that behave as elastic soft solids (Fig. 1b). Transient networks present themselves as fibers that are entangled or bundled, and they form gels that are more fluid in nature (Fig. 1c). Thus, tailoring these initial nucleation modes by altering the amount or type of junction in the network can be utilized to develop materials with unique properties or mechanical behavior.

The incorporation of low molecular weight polymeric species as additives is useful for tuning the nucleation of MGs due to the ability to incorporate complementary functional groups and simultaneously provide structural reinforcement [27–30]. The most effective polymers are rigid in nature; thus, they are either short-chain polymers and/or structures with a rigid backbone conformation [26]. Additionally, structure matching has been used to facilitate interactions between the polymer and MG such that the polymer would effectively absorb along the nucleated network. For example, Rowan et al. utilized a guanosine derivative to form core-sheath fiber networks via polymer–MG interactions [31]. The guanosine-based polymers formed a cooperative assembly with the guanosine molecular gels, and both the gel modulus and shear sensitivity could be tuned via the polymer concentration. To a certain extent, polymers introduced in small quantities were able to interrupt the natural growth of the MG network. For example, an ethylene-vinyl acetate copolymer was utilized to cause mismatched branching in a lanosterol molecular gel by absorbing on the edges of the growing fiber networks [32]. Though polymer additives exist as a minority component, their presence in solution guides the nucleation of self-assembling small molecules, resulting in significant changes in the gel structure and mechanics.

However, guidelines are needed for the development of MGs as additives in composites, which have composition requirements that differ from those in original polymer-additive-based molecular gels. For example, the polymers must exist as the major component or matrix in order to fabricate the composites. Additionally, the polymer chains

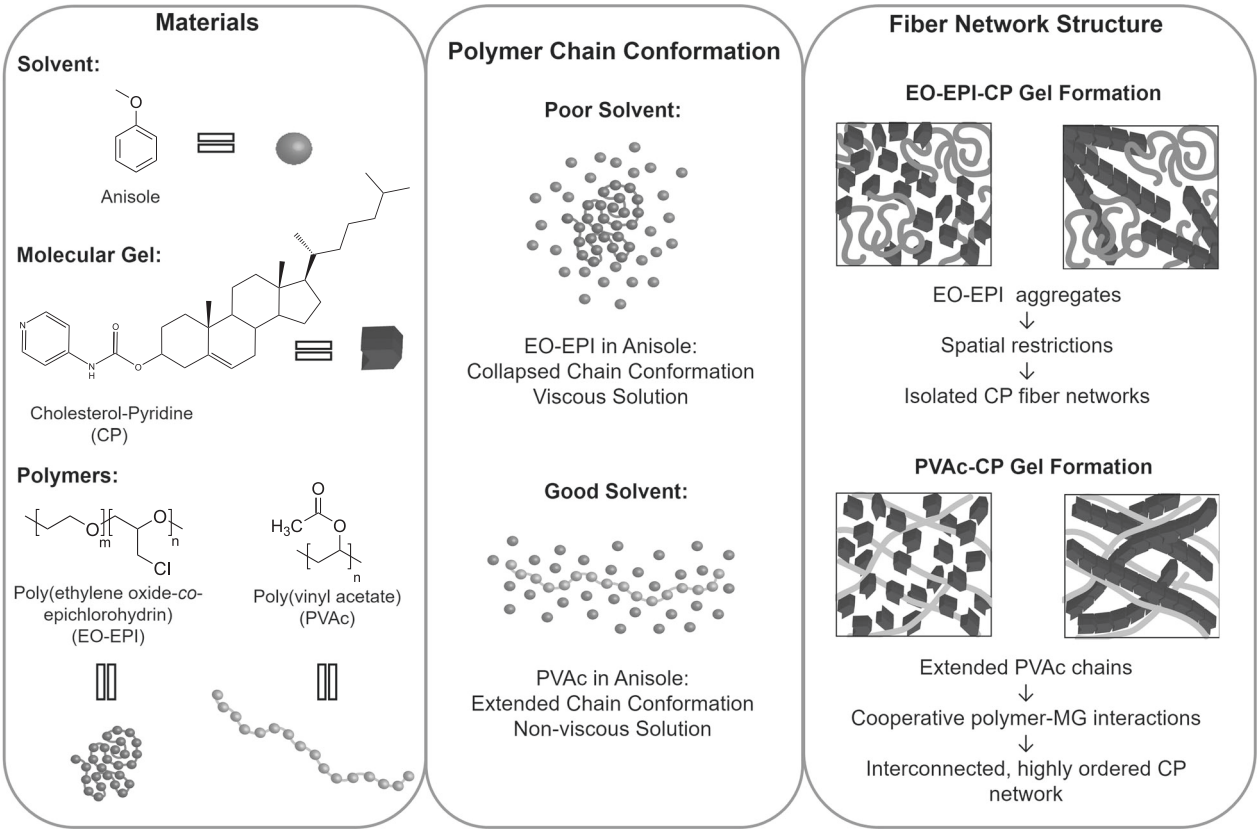

Fig. 2 Chemical structures, schematic representation of polymers in a good vs. a poor solvent, and gel network structure as a function of polymer chain conformation

must be above their entanglement molecular weight to achieve a sufficient mechanical robustness [33]. By utilizing high molecular weight polymers and incorporating the polymers as additives at higher concentrations than those in the molecular gel, the polymer chain conformation will have a significant effect on MG nucleation. Thus, generating MG-reinforced composites requires a re-examination of solution-state polymer–MG interactions with a focus on polymer-solvent properties.

Our group strives to fundamentally examine the introduction of long-chain polymers (above the entanglement MW) to MGs in the gel state. In this work, the effects of long-chain polymers (poly(ethylene oxide-co-epichlorohydrin) (EO-EPI) and poly(vinyl acetate) (PVAc)) on the nucleation and mechanics of MG (cholesterol-pyridine (CP)) are examined. Additionally, two scenarios are explored: one in which gelation occurs in a poor solvent for the polymer chain and another in which gelation occurs in a good solvent. A polymer introduced to a poor solvent will result in a more viscous solution and will have a collapsed chain conformation (Fig. 2), while the polymer in a good solvent will form a low viscosity solution comprised of extended chains that can freely interact with the molecular gel (Fig. 2) [26]. It is expected that these chain behavior differences will influence the solution properties and tailor the interactions between the polymer and the CP molecular gel. Thus, this investigation probes the fundamental interactions between long-chain polymers and MGs through the lens of polymer chain conformation.

To simplify this study, a known cholesterol-pyridine supergelator [34] or an MG capable of gelling a wide variety of solvents at low concentrations and a single solvent (anisole) were chosen to assemble our MG networks (Fig. 2). Changes in the gelation solvent can result in variations in the MG structure; [25] therefore, two polymers (EO-EPI and PVAc) were utilized to demonstrate poor and good solvent conditions in the same gelation solvent. In this work, we explore the changes in MG nucleation in solutions with long-chain polymers and the influence of those changes on the structural and rheological behaviors of the resultant gels. Investigating the solution-state behavior of these systems is expected to expand the understanding of polymer-MG materials and inspire the use of molecular gels as mechanical reinforcements or as stimuli-responsive elements in solid-state polymer composites.

Materials/experimental/characterization

Materials

All chemicals, except for EO-EPI (67% epichlorohydrin), were purchased and used as received from Sigma Aldrich. EO-EPI was obtained from Scientific Polymer Products.

Synthesis of cholesterol-pyridine gelator

A cholesterol-pyridine (CP) gelator was synthesized using a previously described procedure [34]. Briefly, dichloromethane (300 mL) and cholesterol chloroformate (5 g, 0.011 mol) were added to a 500-mL round bottom flask. Then, 4-aminopyridine (2.09 g, 0.022 mol) was added to the flask, and the reaction was stirred at room temperature overnight. The product was then filtered and dried under rotary evaporation to yield an off-white solid. The solid filtrate was rinsed first with acetone and then with hexanes. The remaining product was filtered and dried using vacuum filtration to yield a white solid (4.118 g, 74% yield). The product was characterized using a 600 MHz ^{1}H nuclear magnetic resonance spectrometer (NMR) (Figure S1). ^{1}H NMR (600 MHz, CDCl3) $\delta = 0.68$ (s, 3 H), 0.86–0.87 (m, 6 H), 0.92–2.44 (m, 34 H), 4.60–4.66 (m, 1 H), 5.41–5.42 (m, 1 H), 6.74 (s, 1 H), 7.32 (d, $J = 5.8$ Hz, 2 H), 8.46 (d, $J = 5.8$ Hz, 2 H).

Molecular gel fabrication

The desired amount of CP gelator was added to an empty vial. Then, 2 mL of anisole (control) or a polymer (EO-EPI; PVAc) solution (50 mg mL^{-1} in anisole) was added to the vial. The mixture was heated to 100 °C and stirred until the gelator was fully dissolved. The vial with the gelator solution was then placed on a benchtop to cool under ambient conditions (room temperature, approx. 21 °C). Upon cooling, a loss of solvent flow was observed, and the gel was allowed to equilibrate overnight before testing.

Characterization

Dynamic light scattering (DLS) was conducted on a Wyatt Mobius DLS. The acquisition time was set at 5, 10, and 20 s to ensure that large aggregates were observed. Then, 15 data sets with 5 acquisitions per set were utilized to ensure consistency in the DLS results. The solvodynamic radius with anisole as the selected solvent was calculated utilizing DYNAMICS V7 software, and the autocorrelation functions were exported and replotted using Origin.

Scanning electron microscopy was conducted on either an FEI/Philips XL30 FEG environmental scanning electron microscope (ESEM) or a JSM-7400F high-resolution scanning electron microscope. The ESEM samples were dried in an ambient environment and then imaged without coating. Samples imaged on the JSM-7400F were allowed to dry in an ambient environment and then sputter-coated with an Au/Pd mixture for 15 s before imaging.

Small- and wide-angle X-ray scattering (SAXS/WAXS) experiments were conducted simultaneously in Sector 12ID-B at the X-ray Science Division beamlines at the Advanced Photon Source, Argonne National Laboratory. Static SAXS/WAXS data were acquired from gel samples sealed in an ambient environment in quartz capillaries. In situ gel dissociation data were collected by heating the gel samples in the sealed quartz capillaries in five-degree increments (2 min equilibration) until the diffraction peaks were no longer observed. The sample-to-detector distance and beam size were 1.9 m and 0.08 mm(V) × 0.20 mm(H), respectively, with a wavelength of 0.8856 A (energy 14 KeV). 1D scattering profiles were acquired via azimuthal integration and are presented as the intensity vs. scattering vector (q), where $q = (4\pi/\lambda)\sin\theta$. The domain spacing was calculated using Bragg's law ($n\lambda = 2d\sin\theta$). Small Angle Scattering View (SASView) was utilized to further analyze the gel structures (Figs. S7-S9).

Gel rheological data were collected using a TA Instruments ARES G2 rheometer with parallel plates. Amplitude sweeps were conducted to determine the linear regime for oscillatory frequency sweeps. Frequency sweeps (0.1–100 rad/s) were conducted with an amplitude of 0.01 in order to verify and investigate the gel-like behavior of each system.

Results and discussion

Poor solvent vs. good solvent-polymer choice and chain conformations in anisole

To utilize high molecular weight, preformed polymers in molecular gel fabrication, the gelation solvent must be able to dissolve the polymers and promote gel formation. Anisole was selected as the gelation solvent due to its low toxicity and ability to solubilize a wide variety of polymers [35]. This study focused on molecular gels rather than polymers as additives; thus, utilizing a single polymer concentration reduced the number of variables influencing self-assembly and was sufficient for these preliminary investigations. An EO-EPI or PVAc concentration of 5 wt% (50 mg mL^{-1}) was selected to fabricate solution-cast composites based on prior work [11] and allowed the use of molecular gels with concentrations ranging from 1–3 wt% as the minor component.

It is necessary to understand the solution-state conformations of EO-EPI and PVAc prior to the formation of a

gel network. Their conformations in anisole influence the accessibility of the cholesterol-pyridine gelator and the potential for polymer–MG interactions. Higher molecular weight polymeric species have a greater influence on the solution properties than their rigid, short-chain precursors and are expected to have additional effects on CP nucleation. Additionally, their solubility in the gelation solvent guides the chain conformation and, as a result, affects the ability of the CP molecular gel to interact with EO-EPI and PVAc. Both EO-EPI and PVAc have been utilized as versatile matrices for mechanically enhanced fiber-reinforced composites, inspiring exploration in this investigation [36–40]. Anisole is anticipated to function as a poor solvent for EO-EPI but should readily dissolve PVAc. Both polymers were utilized at the same molecular weight (100,000 g/mol) at a concentration of 5 wt% in anisole.

Dynamic light scattering was utilized to examine the chain conformation of EO-EPI and PVAc at the chosen concentration (5 wt%). Figure 3 shows the intensity autocorrelation function plotted vs. the delay time. The solution containing EO-EPI exhibits long delay times, indicating that the EO-EPI chains form large, microscale aggregates in solution. In contrast, the PVAc solution exhibits very short delay times, signifying that there are little to no aggregates in solution, and the PVAc chains are well-dissolved and extended. Therefore, DLS confirms that anisole is indeed a good solvent for PVAc and a poor solvent for EO-EPI. The aggregated and collapsed chain conformation of EO-EPI is expected to lead to a solution with a higher viscosity, which will likely influence the ability of the molecular gel to form

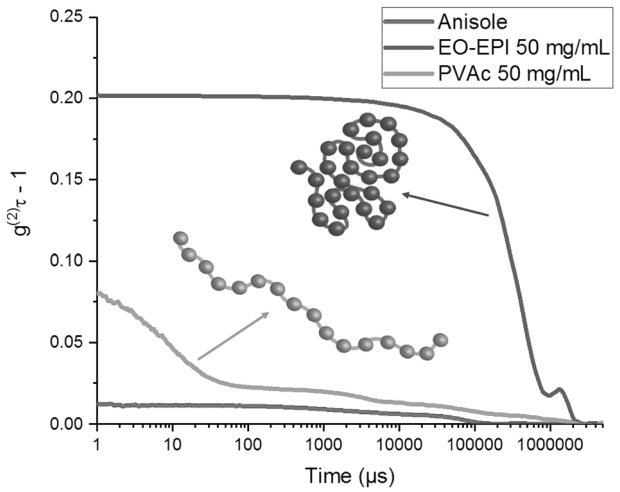

Fig. 3 Dynamic light scattering (DLS) of 50 mg mL^{-1} EO-EPI and PVAc solutions in anisole. EO-EPI exhibits long relaxation times characteristic of large aggregates and PVAc exhibits minimal aggregation, signifying that anisole is a good solvent for PVAc and a poor solvent for EO-EPI

a long-range, interconnected assembly. Conversely, the extended PVAc chains result in a solution with a low viscosity, allowing interactions between the polymer and CP gel. Due to their contrasting solution properties, the solutions of PVAc and EO-EPI were expected to result in dissimilar CP self-assembled fiber networks. To confirm this hypothesis, microscopy was utilized to visualize the CP fiber assemblies resulting from the incorporation of PVAc and EO-EPI.

Formation and visualization of gel-polymer networks through microscopy

To fabricate the gels, either EO-EPI or PVAc was dissolved in anisole at a concentration of 50 mg mL^{-1}, and then, the CP molecular gel was added to the solution. Gelation was achieved by heating the solution until CP dissolved and then cooling the solution to room temperature under ambient conditions. To simplify the discussion of specific samples, the following nomenclature was utilized: E (EO-EPI) or P (PVAc)-CP concentration. For example, a gel sample with EO-EPI and 1 wt% CP is described as E-CP1, and a sample with PVAc is denoted as P-CP1. A summary of the sample nomenclature is included in Fig. 4a.

Changing the CP molecular gel concentration allowed us to examine the influence of EO-EPI or PVAc interactions with the MG content on the network formation. All the formulations withstood the vial inversion test (Fig. 4a), indicating that EO-EPI and PVAc did not impede the formation of the gel network at the chosen concentrations.

Scanning electron microscopy (SEM) was utilized to visually examine the changes in the cholesterol-pyridine self-assembled network. Solution properties can significantly influence the structure of a MG self-assembled network because the solvent actively guides its nucleation [41, 42]. Therefore, differences due to the behavior of PVAc and EO-EPI in anisole are expected to lead to dissimilar fiber networks.

As shown in Fig. 4, SEM revealed fiber networks with significant variations in the long-range network formation. In the absence of EO-EPI or PVAc, the CP gels exhibit highly interconnected fiber networks with significant branching (Figure S2), which is characteristic of fiber networks with permanent nodes, where branching is observed from the tips of the fibers [26]. E-CP gels also exhibit significant branching behavior indicative of assemblies with permanent junctions. However, unlike the nucleation centers in neat CP gels, those in E-CP gels are isolated (Fig. 4b). According to the DLS results, EO-EPI has a collapsed, aggregated structure in anisole; thus, direct interaction of the polymer chains with the small CP molecules is unlikely. Instead, the isolation is likely due to spatial restrictions resulting from the aggregation of EO-EPI

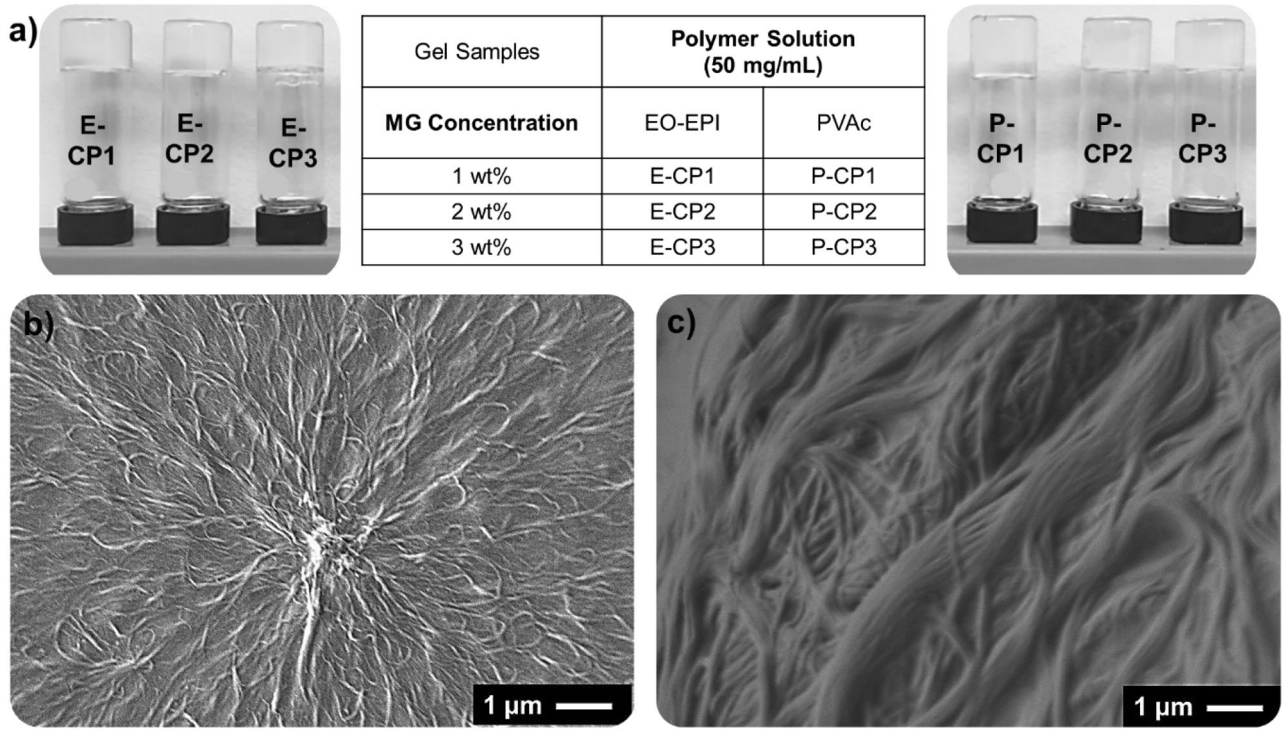

Gel Samples	Polymer Solution (50 mg/mL)	
MG Concentration	EO-EPI	PVAc
1 wt%	E-CP1	P-CP1
2 wt%	E-CP2	P-CP2
3 wt%	E-CP3	P-CP3

Fig. 4 Sample nomenclature, the formation of E-CP and P-CP gels, and the visualization of their self-assembled fiber networks. **a** Demonstration of vial inversion test confirming the formation of gels, and a table summarizing the sample nomenclature. **b** SEM of the E-CP1 gel exhibiting an isolated, highly branched fiber network characteristic of gels comprised of permanent nodes. **c** SEM of the P-CP1 gel exhibiting an interconnected fiber network with fiber wrapping and bundling that is characteristic of gels with transient nodes. Additional SEM images of solution-cast EO-EPI and PVAc, E-CP, and P-CP gels are available in the supplemental information (Figs. S3–S5)

in the poor solvent. The collapsed chains of EO-EPI favor polymer–polymer interactions rather than polymer–anisole attraction, leading to a viscous solution that forces the CP gel molecules to assemble in the space between the aggregates. Therefore, instead of the highly interconnected fiber networks seen in the CP-only gels, isolated branched assemblies are observed.

In contrast, the CP fiber network observed in the PVAc gels exhibits little to no fiber branching. Rather, the P-CP gels show unraveled individual fibers from large bundles. These bundles are composed of individual fibers that appear to be attracted to and overlap with one another (Fig. 4c). This behavior is indicative of the formation of a MG network with transient junctions, which is characterized by overlapping and interconnected or entangled fibers [26]. Anisole is a good solvent for PVAc, signifying that the chains are extended and the solution has a low viscosity. However, although the CP molecules do not have spatial restrictions, the P-CP network is not the same as the cholesterol-pyridine network without any polymer. The change in the assembly could be due to interactions between PVAc and CP molecules during nucleation. PVAc has been shown to directly affect molecular gel networks by adsorbing along the surface of the nucleating gel [32]. To induce this effect, the PVAc chains must be extended and interact favorably with the molecular gel structure via non-covalent interactions. Thus, in addition to molecular design, solvent choice can play a significant role in polymer–MG interactions, especially when utilizing high MW polymers. For this study, both the PVAc chain conformation in anisole and non-covalent interactions between PVAc and the CP gel led to the evolution of transient junctions in the self-assembled fiber network.

For all systems, as the concentration of the CP molecular gel increases, so does the fiber density in the network. For example, the P-CP3 network is so dense that distinguishing between individual fibers was difficult (Figure S2). Additionally, SEM images at lower magnification exhibit directionality in the P-CP3 gels (Figure S5). Interestingly, for the E-CP systems, as the CP concentration increases, so does the interconnectivity and appearance of transient junctions (Figures S2 & S4). This assembly transition indicates that the concentration ratio between EO-EPI and CP can be utilized to influence the nucleation behavior of the self-assembled network. Increasing the CP concentration allows the gel network to overcome the physical barriers produced by EO-EPI aggregates.

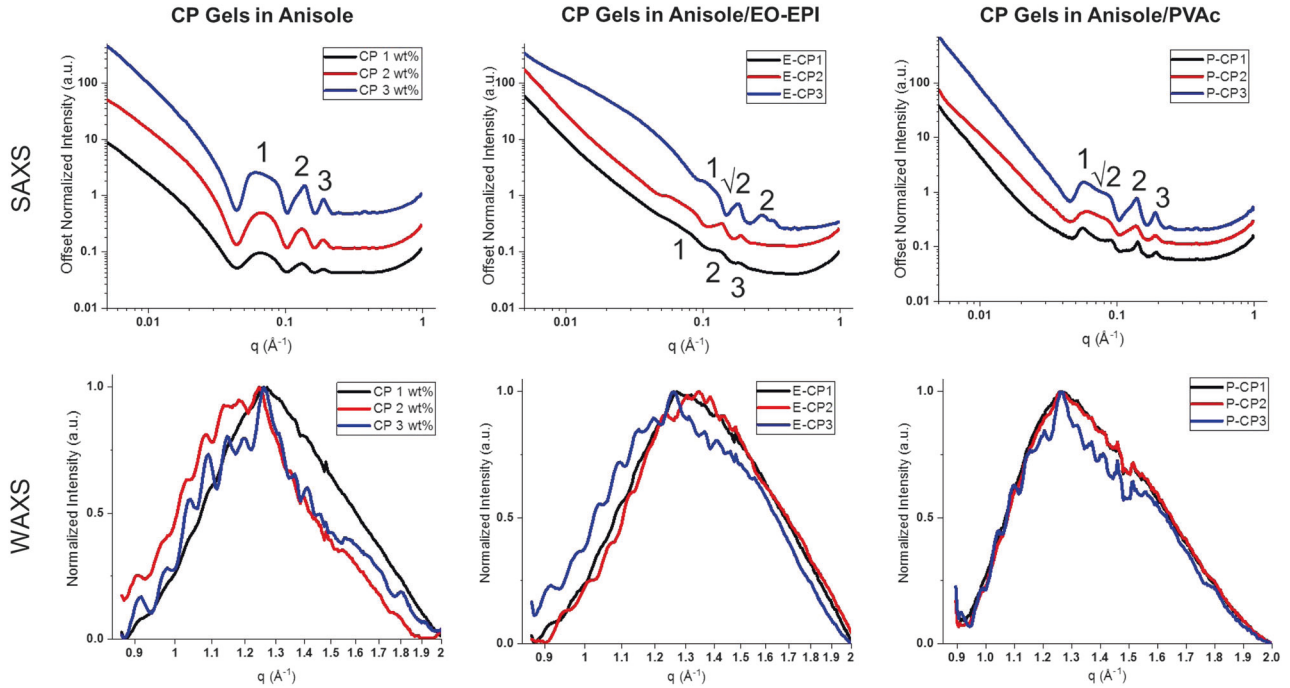

Fig. 5 Static SAXS/WAXS of neat CP, E-CP, and P-CP gels. SAXS reveals changes in assembly as a function of CP concentration for E-CP gels, while the P-CP gels differ from the neat CP gels at all concentrations. WAXS depicts an increase in molecular organization with CP concentration for all samples. P-CP gels exhibit a structural consistency that the other two systems do not, signifying that cooperative interactions between PVAc and CP guide gel nucleation

Investigation of assembly modes through in situ SAXS/WAXS

SEM qualitatively confirmed that EO-EPI and PVAc chain conformations influence the self-assembled fiber network of the cholesterol–pyridine gelator. However, obtaining quantitative descriptions of variations in the gel structure utilizing small- and wide-angle X-ray scattering (SAXS/WAXS) is possible. Several researchers have utilized SAXS/WAXS as tools to understand the molecular assembly of gelators [13, 15, 20, 43–46]. Utilizing these techniques, it is possible to identify the packing arrangements of molecular gels via domain spacing. Additionally, synchrotron beamlines enable the exploration of molecular gels without requiring solvent removal. The ability to observe solvent- swollen polymer-MGs was essential to this investigation because EO-EPI and PVAc may exhibit different conformations in the solid-state vs. in solution.

To quantifiably describe the networks observed via SEM, simultaneous SAXS/WAXS was performed on each gel system (Fig. 5). For SAXS, neat CP gels displayed q spacing ratios of 1:2:3, indicating that the assemblies exist as ordered, lamellar aggregates [25, 47, 48]. Additionally, SASView analysis using a lamellar fit qualitatively agrees with the experimental results (Figure S7). 1D WAXS profiles of solution-state fiber assemblies are not easy to quantify due to the large amorphous halo. However, WAXS can be utilized to qualitatively describe the angstrom-scale molecular structure. For pure CP gels, the area of the amorphous halo decreases with an increase in CP concentration. At higher CP contents, more fiber assembly is observed, which leads to more molecular packing and organization.

The 1D SAXS profiles of E-CP have much lower intensities than those of the pure CP gels; however, the 1 and 2 wt% CP gels also exhibit a ratio of 1:2:3 that is characteristic of lamellar aggregates. In contrast, the E-CP3 gel displays q-spacing ratios of approximately 1:√2:2, representing a disordered rectangular columnar structure [20, 22]. Fitting with SASView qualitatively reveals a mixture of lamellar and columnar structures as the CP concentration increases (Figure S8). This modulation in assembly behavior is induced by the high CP concentration, where the CP molecules overcome the physical barriers of the EO-EPI aggregates and form long-range assemblies. However, the presence of EO-EPI assemblies serves as a physical guide to gelation, leading to columnar structures rather than the lamellar structures observed in neat CP gels. The 1D WAXS profiles of the E-CP gels indicate that the nanoscale molecular organization increases with the increasing CP concentration. The E-CP1 and E-CP2 gels have diffraction peaks that shifted to slightly higher q values, signifying smaller assemblies than those observed in neat CP gels. However, the E-CP3 gel exhibits diffraction

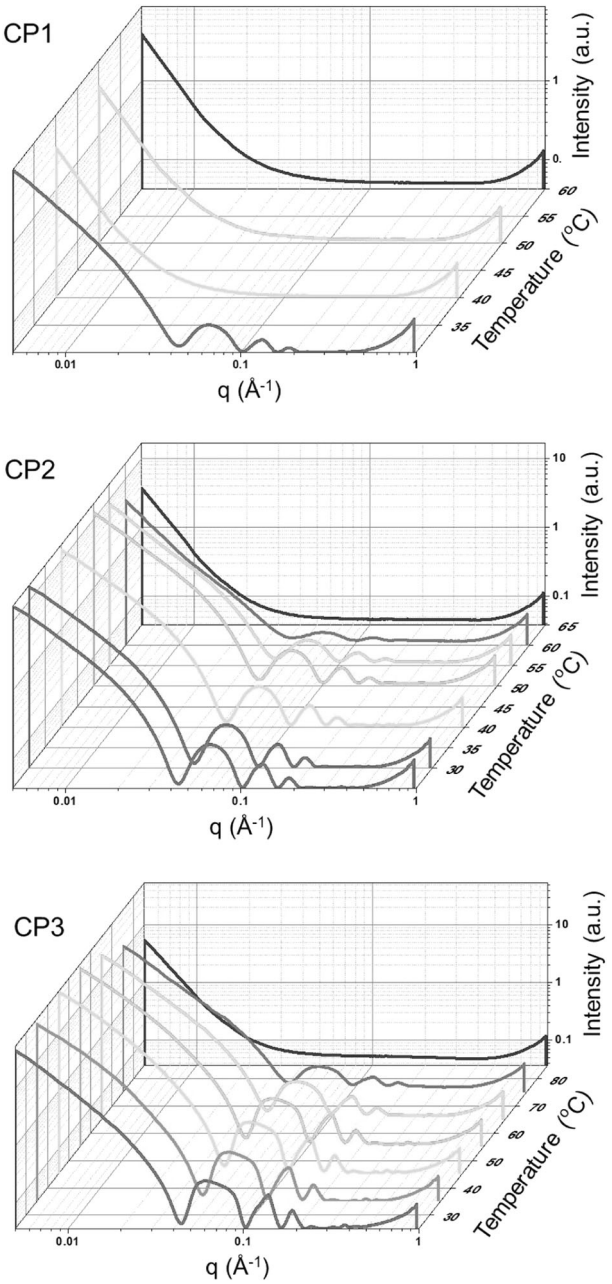

Fig. 6 Temperature-dependent SAXS of neat CP gels

peaks identical to those of the neat CP gels. This observation supports the hypothesis that EO-EPI aggregates spatially restrict the cholesterol–pyridine fiber networks until the CP concentration is high enough to escape the physical boundaries.

At all concentrations, PVAc gels exhibit a 1:√2:2 columnar structure (Fig. 5). This columnar structure is confirmed qualitatively via SASView, but it deviates in the low-q region due to scattering from the PVAc solution (Figure S9). Sharp peaks in the 1D SAXS profiles indicate well-defined domains. PVAc chains are freely extended in anisole and do not act as a spatial barrier to gelation. Therefore, PVAc chains are more likely to have favorable interactions with the CP molecules and actively participate in gel nucleation. This result is supported by the 1D WAXS profile observations (Fig. 5). Unlike neat CP and E-CP gels, the location of the amorphous halos of the P-CP gels are consistent at all CP concentrations, suggesting that the molecular organization of PVAc and CP does not change. Thus, it is inferred that PVAc and CP have some degree of interaction on the molecular level that guides nucleation across multiple length scales.

The dissociation behavior of molecular gels is directly related to their self-assembled network. In situ SAXS can be utilized to observe how a fiber network changes or dissociates as function of temperature. In SAXS, the structure observed is due to the long-range fiber network formed from the molecular assembly of CP gel because EO-EPI and PVAc solutions do not display diffraction peaks in anisole (Figure S6). CP, E-CP, and P-CP gel samples were heated to a temperature at which domains were no longer observed in the 1D SAXS profile, which indicates their dissociation temperature ($T_{g,dis}$).

First, it is necessary to establish the dissociation behavior of the CP gel independent of polymer additives. Temperature-dependent SAXS curves of cholesterol–pyridine MGs in anisole displayed expected gel dissociation trends. Both the gel dissociation temperature and peak intensity increase proportionally to the CP gel concentration ($T_{g,dis}$ CP1 = 40 °C, $T_{g,dis}$ CP2 = 65 °C, $T_{g,dis}$ CP3 = 85 °C) (Fig. 6).

Despite similarities in packing structure between neat CP gels and E-CP gels, the EO-EPI gels display unexpected fluctuations in their dissociation behavior as the CP concentration changes. The E-CP1 gel exhibits an uncharacteristically high dissociation temperature with structural features visible up to 125 °C (Fig. 7). The E-CP2 gel, which has a higher CP content, exhibits a much lower dissociation temperature than its 1 wt% counterpart, matching the $T_{g,dis}$ of the 2 wt% neat CP gel (65 °C). Additionally, the E-CP3 gel has a higher dissociation temperature than the 3 wt% neat CP gel (95 °C) (Fig. 7). Thus, in addition to visual confirmation through SEM, the concentration ratio of EO-EPI to CP is shown to greatly affect the self-assembled fiber network. The concentration ratio influences gel formation to the extent that a dissimilar dissociation behavior is observed compared to the pure CP gels despite both systems exhibiting similar domain spacings. These observations are particularly interesting because the E-CP gels have lower scattering intensities, but in two instances, they exhibit higher dissociation temperatures than pure CP gels. It is hypothesized that the cause for the high dissociation temperature of the E-CP1 gels is due to the solution behavior of EO-EPI, which causes a confinement effect [49]. At lower CP concentrations, the CP gel molecules are concentrated

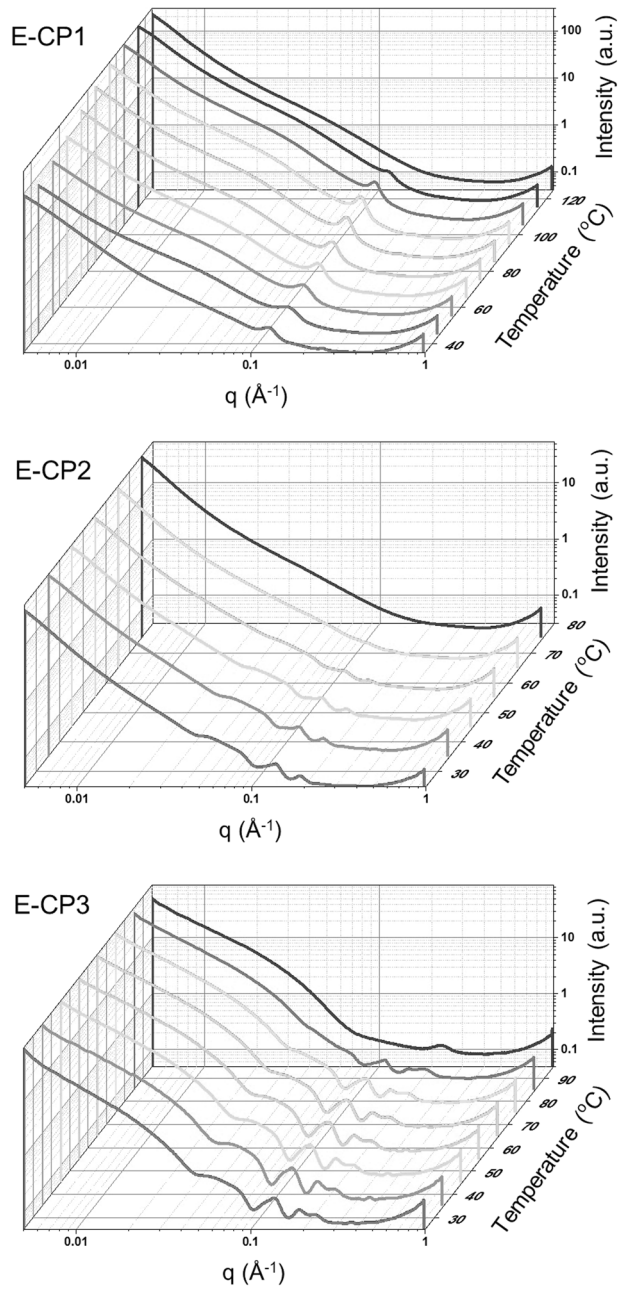

Fig. 7 Temperature-dependent SAXS of E-CP gels

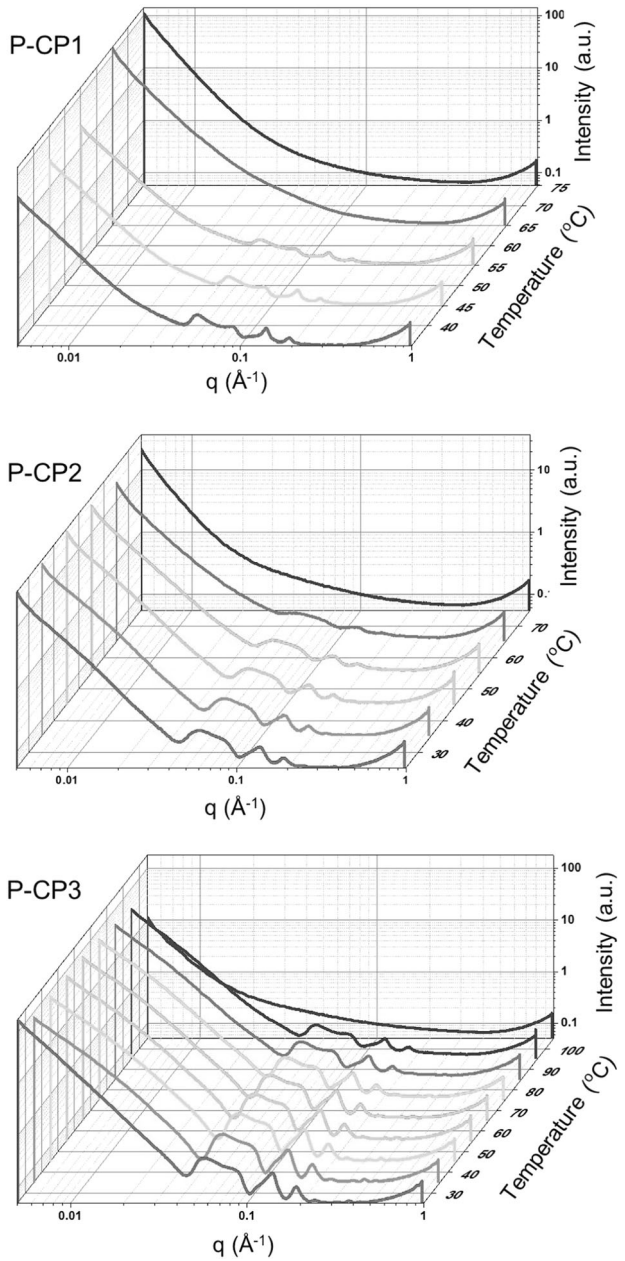

Fig. 8 Temperature-dependent SAXS of P-CP gels

into isolated fiber arrangements due to spatial restrictions imposed by EO-EPI aggregates. These arrangements lead to assemblies of highly concentrated CP fiber networks, resulting in higher dissociation temperatures. The isolated fiber networks displayed in the microscopy (Fig. 4b) support this conclusion. However, at higher CP contents, the cholesterol–pyridine gel network overcomes the spatial restrictions imposed by the EO-EPI chains, leading to a long-range assembly. When the CP concentration increases, the confinement effect no longer exists, and the dissociation temperature of the E-CP2 gel matches that of the CP2 gel. In E-CP3 gels, the EO-EPI aggregates are beneficial to the network stabilization. The EO-EPI spatial boundaries coupled with the highest CP concentration result in a self-assembled structure similar to that of the P-CP gels (Fig. 5). Thus, both changes in the peak ratio and an increase in the dissociation temperature are observed.

Despite the difference in the network structure evidenced by the domain spacing in the static SAXS/WAXS profiles, P-CP systems also exhibit the expected trend of increased dissociation temperatures proportional to the CP concentration. However, the P-CP gels have significantly higher dissociation temperatures compared to those of the

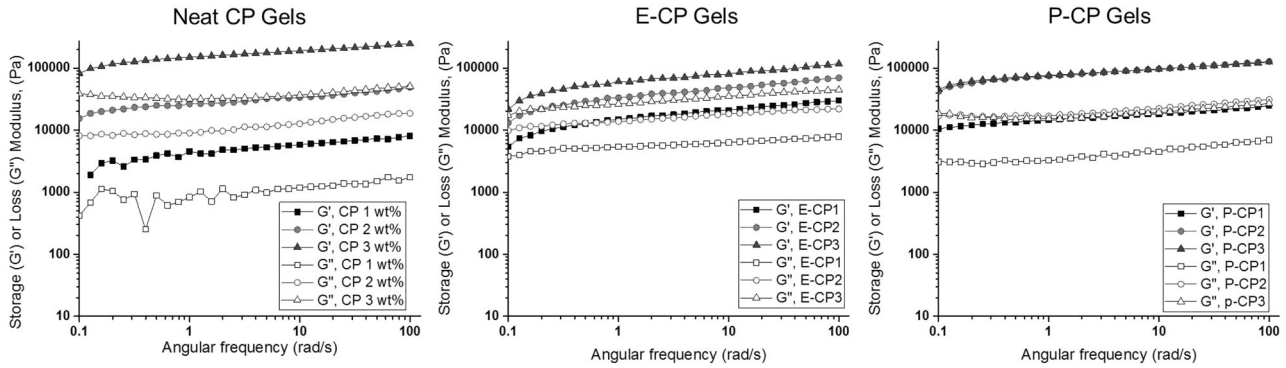

Fig. 9 Rheological behavior of neat CP, E-CP, and P-CP gels

pure CP gels (P-CP1 = 65 °C, P-CP2 = 75 °C, P-CP3 = 105 °C) (Fig. 8). We propose that this stabilization, which is reflected as a fourth-order peak in the 1D SAXS profile, represents a synergistic interaction between the CP molecular gel and PVAc. This synergism should result in structural reinforcement via absorption on the nucleating fiber surface [26, 32, 50]. As shown in Fig. 5, the P-CP gels exhibit sharp peaks in the 1D WAXS profile, indicating significant crystallographic order even in high-q regions, corresponding to angstrom-scale molecular interactions. Additionally, even the amorphous halo remains largely consistent, increasing in peak intensity proportional to the CP concentration (Fig. 5). In contrast to the type of interactions in EO-EPI gels, this evidence indicates cooperation between PVAc polymer chains and the self-assembled CP fiber network.

Rheological investigation of solution-state mechanics

Qualitative and quantitative descriptions of the effects of the solution behavior of PVAc and EO-EPI on CP gel network structures were achieved utilizing light scattering, microscopy, and X-ray scattering techniques, and these structural characteristics are expected to influence the mechanical behavior of the gels. Rheological investigation of the polymer-infused gels was utilized to correlate the CP network structures to the gel mechanics. Rheological gel-like behavior (G′>G″) was observed for all sample formulations. For the neat CP gels and E-CP gels, the gel strength increases with increasing concentration (Fig. 9). However, the separation between G′ and G″ is less for the EO-EPI gels, indicating the gel network is more viscous in nature (Fig. 9). In these molecular gel networks, the polymer solution is the major component. Thus, the high viscosity of an EO-EPI solution in anisole leads to a gel network with a high loss modulus. The E-CP1 gel exhibits the highest separation of G′ and G″, which is evidence of a more elastic gel network [51, 52], supporting the hypothesis that CP molecules are concentrated in isolated areas of the gel network. While the isolated CP fibers result in a high elasticity and dissociation temperature, as shown in the temperature-dependent SAXS, the formed gels are much weaker due to the lack of interconnected fiber assemblies. Visualization of these assemblies via SEM depicted isolated, densely branched structures separated by the polymer matrix (Fig. 5). Therefore, there is a distinct interfacial boundary between the EO-EPI aggregates and the CP gel structures, where the EO-EPI chains act as viscous barriers that prevent additional reinforcement via fiber connectivity.

In contrast to the characteristics of neat CP and E-CP gels, the strength of the P-CP initially increases with increasing CP and is identical for 2 and 3 wt% CP (Fig. 9). This trend is characteristic of gels with polymer additives that follow the path of the gel assembly or that directly interact with the self-assembling small molecule [31, 51]. The separation between G′ and G″ is consistent despite the changes in concentration, which is also evidence that polymer–MG interactions guide the nucleation process. Although the dissociation temperature increases with increasing CP concentration, the same is not true of the gel strength, which likely indicates that the materials reach a saturation limit beyond which the PVAc chains can no longer be incorporated into the entire CP network structure. As shown in the SEM and SAXS/WAXS results, the P-CP gel networks do not change structure but increase in their overall fiber content. Past a certain point, the fibers become nearly indistinguishable from each other, and the addition of more CP molecules has no significant effect on the mechanical behavior.

Conclusions and future outlook

In this work, high molecular weight polymers were introduced to low molecular weight gels to explore the effect of the polymer chain conformation on the solution properties and gel formation. While anisole served as a good solvent for PVAc, it was a poor solvent for EO-EPI, leading to a

viscous solution consisting of large EO-EPI aggregates. These large aggregates produced isolated fiber networks in contrast to the highly interconnected fiber assemblies shown in neat CP gels. Though the E-CP gels originally exhibited the same permanent network structure, the CP concentration could be utilized to overcome the spatial boundaries and introduced more transient junctions. The change in structure was confirmed by SAXS/WAXS, highlighting a transition from lamellar aggregates to columnar arrangements. The imposed spatial restrictions on the nucleating CP molecules in the E-CP gels also led to unexpected dissociation behavior. While EO-EPI beneficially enhanced the dissociation temperature by concentrating and guiding the CP networks, it negatively influenced the gel mechanics, resulting in highly viscous gels with lower moduli than the gels without polymer additives.

At all concentrations, the P-CP gels exhibited via SEM a fiber network comprised primarily of transient junctions. Since PVAc displayed an extended chain conformation behavior in DLS, the difference in structure was likely due to cooperative interactions between the PVAc chains and the assembling CP molecules. Favorable interactions in the P-CP gels were confirmed through columnar arrangements in SAXS and structural consistency in WAXS and resulted in gels with higher dissociation temperatures. Additionally, the elastic modulus of the P-CP gel remained the same for composition ranging from 2 to 3 wt%, signifying that no additional structural benefit was provided by increasing the CP concentration. SEM confirmed that the materials were reaching a saturation limit because the gels did not change their structure but instead formed a denser network until the fibers were nearly indistinguishable. Despite the saturation of the fiber network, the P-CP gels exhibited a higher elasticity than the E-CP gels due to the lower viscosity of the PVAc solution compared to that of the EO-EPI solution.

From this work, it is evident that polymer chain conformation plays a significant role in molecular gel network formation. Polymer solution behavior affects the permanent or transient nature of the MG, the crystallographic structure, and the dissociation behavior of a molecular gel. As a result, these structural characteristics influence the gel mechanics. Since the hierarchical structure of an additive in a polymer composite significantly influences the mechanical properties, the impact of the polymer chain conformation on gel nucleation should be considered when designing MG–polymer composites. In future work, we intend to explore the characteristics of the E-CP and P-CP gel structures and mechanics in solid-state polymer nanocomposites.

Acknowledgements The authors acknowledge financial support from the DuPont Young Professor Grant. S. Alexander would like to thank the NSF Graduate Research Fellowship for financial support. This research used resources from the Advanced Photon Source, a U. S. Department of Energy (DOE) Office of Science User Facility operated for the DOE Office of Science by Argonne National Laboratory under Contract no. DE-AC02-06CH11357. This work made use of the MRSEC Shared Experimental Facilities at MIT, supported by the National Science Foundation under award number DMR-14-19807. Additionally, this work utilized the Advanced Materials Characterization Laboratory (AMCL) and the Keck Center for Advanced Microscopy and Microanalysis (Keck CAMM) at the University of Delaware for dynamic light scattering and scanning electron microscopy, respectively. This work also benefited from the use of the SasView application, originally developed under NSF award DMR-0520547. SasView contains code developed with funding from the European Union's Horizon 2020 research and innovation programme under the SINE2020 project, Grant agreement no 654000.

References

1. Dagnon KL, Shanmuganathan K, Weder C, Rowan SJ. Water-triggered modulus changes of cellulose nanofiber nanocomposites with hydrophobic polymer matrices. Macromolecules. 2012;45:4707–15.
2. Paul DR, Robeson LM. Polymer nanotechnology: nanocomposites. Polymer. 2008;49:3187–204.
3. Luo H, Hu J, Zhu Y. Path-dependent and selective multi-shape recovery of a polyurethane/cellulose-whisker nanocomposite. Mater Lett. 2012;89:172–5.
4. Wu T, Frydrych M, Kelly KO, Chen B. Poly(glycerol sebacate urethane)–cellulose nanocomposites with water-active shape-memory effects. Biomacromolecules. 2014;15:2663–71.
5. Huang ZM, Zhang YZ, Kotaki M, Ramakrishna S. A review on polymer nanofibers by electrospinning and their applications in nanocomposites. Compos Sci Technol. 2003;63:2223–53.
6. Jordan J, Jacob KI, Tannenbaum R, Sharaf MA, Jasiuk I. Experimental trends in polymer nanocomposites—a review. Mater Sci Eng A. 2005;393:1–11.
7. Cudjoe E, et al. Biomimetic reversible heat-stiffening polymer nanocomposites. ACS Cent Sci. 2017;3:886–94.
8. Sattar R, Kausar A, Siddiq M. Advances in thermoplastic polyurethane composites reinforced with carbon nanotubes and carbon nanofibers: a review. J Plast Film Sheet. 2014;31:186–224.
9. De Leon AC, et al. High performance polymer nanocomposites for additive manufacturing applications. React Funct Polym. 2016;103:141–55.
10. McNally, T, Potschke, P. Polymer-carbon nanotube composites. Woodhead Publishing Limited: Cambridge; 2011.
11. Stone DA, Wilusz E, Zukas W, Wnek G, Korley LTJ. Mechanical enhancement via self-assembled nanostructures in polymer nanocomposites. Soft Matter. 2011;7:2449–55.
12. Weiss, RG, Terech, P. Molecular gels: materials with self-assembled fibrillar networks. Springer: Netherlands; 2006.
13. Cui J, Shen Z, Wan X. Study on the gel to crystal transition of a novel sugar-appended gelator. Langmuir. 2010;26:97–103.
14. Reddy SMM, Shanmugam G, Duraipandy N, Kiran MS, Mandal AB. An additional fluorenylmethoxycarbonyl (Fmoc) moiety in di-Fmoc-functionalized L-lysine induces pH-controlled ambidextrous gelation with significant advantages. Soft Matter. 2015;11:8126–40.
15. Delbecq F, Kaneko N, Endo H, Kawai T. Solvation effects with a photoresponsive two-component 12-hydroxystearic acid-azobenzene additive organogel. J Colloid Interface Sci. 2012;384:94–98.
16. Pozzo J-L, Clavier GM, Desvergne J-P. Rational design of new acid-sensitive organogelators. J Mater Chem. 1998;8:2575–7.

17. Roy S, et al. Dramatic specific-ion effect in supramolecular hydrogels. Chem A Eur J. 2012;18:11723–31.
18. Yu, X, Chen, L, Zhang, M, Yi, T. Low-molecular-mass gels responding to ultrasound and mechanical stress: towards self-healing materials. Chem Soc Rev. 2014;43:5346–71.
19. Kiyonaka S, Zhou S-L, Hamachi I. pH-responsive phase transition of supramolecular hydrogel consisting of glycosylated amino acetate and carboxylic acid derivative. Supramol Chem. 2003;15:521–8.
20. Terech, P, Ostuni, E, Weiss, RG. Structural study of cholesteryl anthraquinone-2-carboxylate (CAQ) physical organogels by neutron and X-ray small angle scattering. J Phys Chem. 1966;100:3759–66.
21. Sakurai, K, Kimura, T, Gronwald, O, Inoue, K, Shinkai, S. A hexagonally organized elemental supramolecular structure of a sugar-appended organogelator observed by synchrotron X-ray source. Chem. Lett. 2001:746–7.
22. Lim GS, Jung BM, Lee SJ, Song HH, Kim C. Synthesis of polycatenar-type organogelators based on chalcone and study of their supramolecular architectures. Chem Mater. 2007;19: 460–7.
23. Xing P, Chen H, Bai L, Hao A, Zhao Y. Superstructure formation and topological evolution achieved by self-organization of a highly adaptive dynamer. ACS Nano. 2016;10:2716–27.
24. Babu TM, Prasad E. Charge-transfer-assisted supramolecular 1 D nanofibers through a cholesteric structure-directing agent: self-assembly design for supramolecular optoelectronic materials. Chem A Eur J. 2015;1599:11972–5.
25. Links, DA, Dhinakaran, MK, Das, TM. Studies on a novel class of triaryl pyridine N-glycosylamine amphiphiles as super gelators. Org Biomol Chem. 2012:2077–83. https://doi.org/10.1039/c2ob06834f
26. Li JL, Liu XY. Architecture of supramolecular soft functional materials: from understanding to micro-/nanoscale engineering. Adv Funct Mater. 2010;20:3196–216.
27. Cornwell DJ, Smith DK. Expanding the scope of gels—combining polymers with low-molecular-weight gelators to yield modified self-assembling smart materials with high-tech applications. Mater Horiz. 2015;2:279–93.
28. Pont G, Chen L, Spiller DG, Adams DJ. The effect of polymer additives on the rheological properties of dipeptide hydrogelators. Soft Matter. 2012;8:7797.
29. Adhia YJ, Schloemer TH, Perez MT, McNeil AJ. Using polymeric additives to enhance molecular gelation: impact of poly(acrylic acid) on pyridine-based gelators. Soft Matter. 2012;8:430.
30. Zhang Z, et al. Enhancing gelation ability of a dendritic gelator through complexation with a polyelectrolyte. Chem A Eur J. 2009;15:2352–61.
31. Way AE, et al. Enhancing the mechanical properties of guanosine-based supramolecular hydrogels with guanosine-containing polymers. Macromolecules. 2014;47:1810–8.
32. Liu XY, et al. Creating new supramolecular materials by architecture of three-dimensional nanocrystal fiber networks. J Am Chem Soc. 2002;124:15055–63.
33. Landel, RF, Nielsen, LE. Mechanical properties of polymers and composites. CRC Press: New York, USA; 1993.
34. Malik S, Kawano Sichiro, Fujita N, Shinkai S. Pyridine-containing versatile gelators for post-modification of gel tissues toward construction of novel porphyrin nanotubes. Tetrahedron. 2007;63:7326–33.
35. Anisole. National Center for Biotechnology Information, PubChem Compound Database; CID=7519, https://pubchem.ncbi.nlm.nih.gov/compound/7519 (accessed May 2, 2018).
36. Geng S, Haque MMU, Oksman K. Crosslinked poly(vinyl acetate) (PVAc) reinforced with cellulose nanocrystals (CNC): structure and mechanical properties. Compos Sci Technol. 2016;126:35–42.
37. Wanasekara ND, Matolyak LE, Korley LTJ. Tunable mechanics in electrospun composites via hierarchical organization. ACS Appl Mater Interfaces. 2015;7:22970–9.
38. Qiu X, Hu S. 'Smart' materials based on cellulose: a review of the preparations, properties, and applications. Mater. 2013;6:738–81.
39. Miao C, Hamad WY. Cellulose reinforced polymer composites and nanocomposites: a critical review. Cellulose. 2013;20:2221–62.
40. Alexander SLM, Korley LTJ. Tunable hygromorphism: structural implications of low molecular weight gels and electrospun nanofibers in bilayer composites. Soft Matter. 2017;13:283–91.
41. Yan N, et al. Pyrenyl-linker-glucono gelators. Correlations of gel properties with gelator structures and characterization of solvent effects. Langmuir. 2013;29:793–805.
42. Huang Y, et al. Unusual C − I ··· O halogen bonding in triazole derivatives: gelation solvents at two extremes of polarity and formation of superorganogels. Langmuir. 2017;33:311–21.
43. Chakraborty P, Bairi P, Roy B, Nandi AK. Improved mechanical and electronic properties of co-assembled folic acid gel with aniline and polyaniline. ACS Appl Mater Interfaces. 2014;6:3615–22.
44. Zhang Y, et al. Electrospun biomimetic nanocomposite nanofibers of hydroxyapatite/chitosan for bone tissue engineering. Biomaterials. 2008;29:4314–22.
45. Xue P, et al. Functional organogel based on a salicylideneaniline derivative with enhanced fluorescence emission and photochromism. Chem A Eur J. 2007;13:8231–9.
46. Takeno H, Mochizuki T. A structural development of an organogel explored by synchrotron time-resolved small-angle X-ray scattering. Colloid Polym Sci. 2013;291:2783–9.
47. Wu Y, et al. Photoinduced reversible gel–sol transitions of dicholesterol-linked azobenzene derivatives through breaking and reforming of van der Waals interactions. Soft Matter. 2011;7:716–21.
48. Luo X, Li Z, Xiao W, Wang Q, Zhong J. Self-assembled organogels formed by monochain derivatives of ethylenediamine. J Colloid Interface Sci. 2009;336:803–7.
49. Chen W, Yang Y, Lee CH, Shen AQ. Confinement effects on the self-assembly of 1,3:2,4-di-p-methylbenzylidene sorbitol based organogel. Langmuir. 2008;24:10432–6.
50. Chakraborty P, Roy B, Bairi P, Nandi AK. Improved mechanical and photophysical properties of chitosan incorporated folic acid gel possessing the characteristics of dye and metal ion absorption. J Mater Chem. 2012;22:20291.
51. Li JL, Yuan B, Liu XY, Wang XG, Wang RY. Kinetically controlled homogenization and transformation of crystalline fiber networks in supramolecular materials. Cryst Growth Des. 2011;11:3227–34.
52. Sangeetha NM, Maitra U. Supramolecular gels: functions and uses. Chem Soc Rev. 2005;34:821–36.